Energy Dissipation of Vortices in Single Crystal of Layered Superconductors Bi2SrCaCu2O8 + δ and κ -(BEDT-TTF)2Cu(NCS)2 under Magnetic Fields

Bulletin of Osaka Prefecture University
Series A, Vol. 46, No. 1, 1997, pp.47−54

Energy Dissipation of Vortices in Single Crystal of Layered Superconductors $Bi_2Sr_2CaCu_2O_{8+\delta}$ and κ-$(BEDT\text{-}TTF)_2Cu(NCS)_2$ under Magnetic Fields

Hirofumi NIIMI*, Kazuo INOUE*, Shuichi KAWAMATA**, Kiichi OKUDA**,
Takahiko SASAKI*** and Naoki TOYOTA****

(Received July 11, 1997)

Energy dissipation of vortices in layered superconductors $Bi_2Sr_2CaCu_2O_{8+\delta}$ and κ-$(BEDT\text{-}TTF)_2Cu(NCS)_2$ was investigated by the free torsional damping oscillation in magnetic fields up to 9 kOe in the temperature range from 1.5 K to the superconducting transition temperature T_c. The torque and damping coefficients were obtained as a function of the magnetic field and the temperature. A large anisotropy of damping and torque coefficients were found and explained by assuming a model of two dimensional vortex pancakes.

1. Introduction

The superconducting properties of the high-T_c copper oxides are characterized by the large anisotropy originated from the layered structure in which the conducting CuO_2 layers and the insulating blocking layers are alternately piled up. The crystal structure of the oxide superconductors are reduced from the modification of the perovskite structure. On the other hand, the organic superconductors including the Bisethylenedithio-tetrathiafulvalen (BEDT-TTF) molecules are regardless of the perovskite structure. However, their superconducting properties are characteristic of the two dimensional superconductor as well as the high-T_c copper oxides because of the layered structure consisting of the conducting BEDT-TTF molecules layer and the insulating anion layer.

A lot of new phenomena concerning about the magnetic field H vs. temperature T phase diagram has been investigated in these layered superconductors both by theoretical and experimental researchers[1−6]. Especially, the vortex lattice melting[7], the anomalous depinning and the dimensional crossover of vortex pancakes[8] attract mach attention. In order to study the vortex dynamics, the study of the energy dissipation accompanied by the vortex motion are important. The typical method to study the energy dissipation is an ac susceptibility measurement. In the case of the ac susceptibility measurement, the response to the modulation of the flux line density is observed. This corresponds to the compressibility measurement for the vortex lattice. On the other hand, the response to the tilting of the flux line is observed in the case of the torsional oscillation. That corresponds to the tilt modulus measurement for the vortex lattice. Farrell et al. found the dissipation peaks in the reversible region of $YBa_2Cu_3O_{7-\delta}$ (YBCO)[9]. They claimed that the peaks reveal the melting transition.

In this paper, low frequency torsional oscillation measurement is applied to two kinds of layered superconductors: the high-T_c copper oxide superconductor, $Bi_2Sr_2CaCu_2O_{8+\delta}$ (Bi2212), and the organic salt superconductor, κ-$(BEDT\text{-}TTF)_2Cu(NCS)_2$. They are typical two dimensional superconductors for each material group. The anisotropy parameter defined by the square root of ratio of the in-plane effective mass to that perpendicular to the conducting plane, γ, is reported as $\gamma=55$ to 220 for Bi2212[10,11] and $\gamma=200$ to 350 for κ-$(BEDT\text{-}TTF)_2Cu(NCS)_2$[12,13]. The conducting layer lies in the ab-plane for Bi2212 and in the bc-plane for κ-$(BEDT\text{-}TTF)_2Cu(NCS)_2$. The common

* Graduate Student, Department of Physics and Electronics, College of Engineering
** Department of Physics and Electronics, College of Engineering
*** Institute for Material Research, Tohoku University, Aoba-ku, Sendai 980-77, Japan
**** Research Institute for Advanced Science and Technology

properties for the vortex dynamics in the H-T phase diagram of the layered superconductors are reported.

2. Experimental

Figure 1 shows the schematic diagram of oscillation system. Free torsional oscillator has been made up by hanging a inertia disk of a brass cylinder and a quartz rod from the suspension wire of tungsten. Rotational oscillation is detected optically. The rotational oscillation axis is perpendicular to the applied field. The oscillation period is about 3 seconds in zero field.

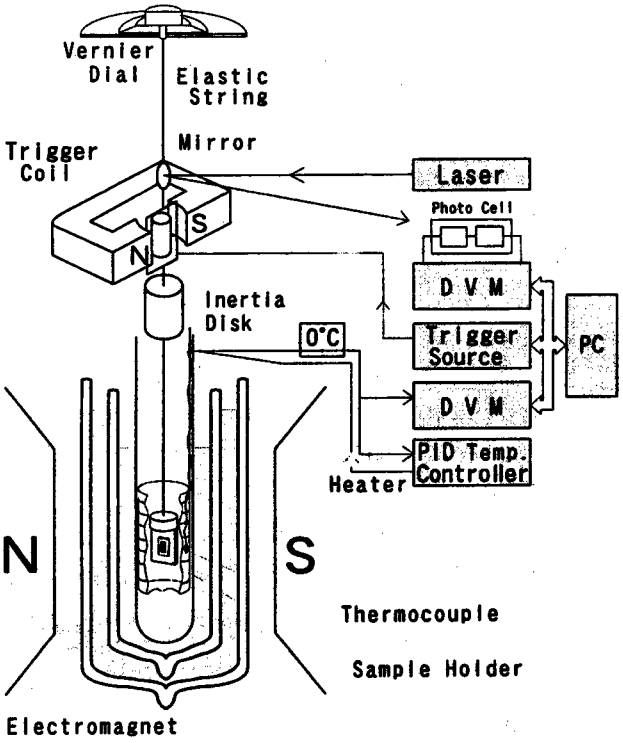

Fig. 1. The schematic diagram of oscillation system.

The equation of motion of the torsional oscillator is described as

$$I\frac{d^2\theta}{dt^2}+\eta\frac{d\theta}{dt}+K\theta=0, \qquad (1)$$

where I, θ, t, η and K represent the moment of the inertia of the oscillating system (I=5.14 g•cm^2), rotational angle, time, a damping constant and a torque coefficient, respectively. η and K are given by the summation of the contribution due to the oscillator apparatus itself and that due to the sample as

$$\eta=\eta_0+\eta_{sample},\quad K=k_0+k_{sample}, \qquad (2)$$

where η_0, η_{sample}, k_0 and k_{sample} represent the damping coefficient by the oscillator apparatus, that by the sample, the torque coefficient by the restoring force of the suspension wire (k_0=0.412 dyn•cm/degrees) and that generated by the sample under magnetic fields, respectively. Below T_c and under magnetic fields, the oscillation is damped by the energy dissipation of vortices. The solution of Eq.(1) becomes

$$\theta(t)=\theta_0\exp(-t/\tau)\cos(\omega t+\delta), \qquad (3)$$

where θ_0 and δ are the initial angle and the initial phase, respectively. Initial declined angle of the crystal axis from the direction of the magnetic field was less than 1 degree for all kinds of measurement. The decay time τ and frequency ω are given by

$$\tau=\frac{2I}{\eta},\quad \omega=\sqrt{(K/I)-(\eta/2I)^2}. \qquad (4)$$

Experimental values for τ and ω are obtained by fitting $\theta(t)$ at each temperature and magnetic field by means of least-square program of Eq.(3). In zero field, τ and ω depend only on η_0 and k_0 at each temperature. η_{sample} is obtained by subtracting $1/\tau$ in zero field from that in magnetic fields. k_{sample} is also obtained by using k_0 data from the zero field measurement at the same temperature.

The Bi2212 single crystals were prepared by the traveling solvent floating zone method. These samples are annealed at 618 ℃ for 70 hour to homogenize the oxygen distribution in the compound. The superconducting transition temperature and the transition width are T_c=87.4 K and ΔT_c = 0.8 K, respectively. Three samples with suitable size has been used in the measurements. The samples is in the form of thin flat plates of dimensions: (a) 2.5×1.3×0.02, (b) 1×0.5×0.02, (c) 0.5×0.5×0.003 mm^3.

κ-(BEDT-TTF)$_2$Cu(NCS)$_2$ single crystal was grown by an electrochemical oxidation method[14]. The sample is also in the form of flat plate of dimension: 2.5×1.4×0.2 mm^3 weighting 0.6 mg. The superconducting transition temperature is T_c=9.7 K.

Four kinds of experiments in different field configuration and cooling method were done for each sample of Bi2212 and κ-(BEDT-TTF)$_2$Cu(NCS)$_2$. For each

compound, the measurements have been done for both configuration of the magnetic field perpendicular to the layer plane and that parallel to the layer plane, and for each field configuration, the measurements have been done in zero fields cooling and in field cooling. The experimental conditions are summarized in Table 1. In Bi2212 case, ZFC and FC indicate cooling down from 100 K to 4.2 K through T_c in zero field and in a given applied field, respectively. In κ-(BEDT-TTF)$_2$Cu(NCS)$_2$ case, ZFC FC indicate cooling down from the temperature above 20 K to 1.5 K through T_c in zero field and in a given applied field, respectively.

Table 1 Experimental condition

	Sample	Cooling method	Magnetic field direction for $\theta = 0°$
Bi-1	$Bi_2Sr_2CaCu_2O_{8+\delta}$	ZFC	$H\perp$ conducting layer($H\perp$ ab)
Bi-2	$Bi_2Sr_2CaCu_2O_{8+\delta}$	FC	$H\perp$ conducting layer($H\perp$ ab)
Bi-2	$Bi_2Sr_2CaCu_2O_{8+\delta}$	ZFC	H// conducting layer(H// ab)
Bi-2	$Bi_2Sr_2CaCu_2O_{8+\delta}$	FC	H// conducting layer(H// ab)
ET-1	κ-(BEDT-TTF)$_2$Cu(NCS)$_2$	ZFC	$H\perp$ conducting layer($H\perp$ bc)
ET-2	κ-(BEDT-TTF)$_2$Cu(NCS)$_2$	FC	$H\perp$ conducting layer($H\perp$ bc)
ET-3	κ-(BEDT-TTF)$_2$Cu(NCS)$_2$	ZFC	H// conducting layer(H// bc)
ET-4	κ-(BEDT-TTF)$_2$Cu(NCS)$_2$	FC	H// conducting layer(H// bc)

3. Results and discussion

3.1. $Bi_2Sr_2CaCu_2O_{8+\delta}$

Typical examples of the oscillations are shown in Fig. 2 (a) at T=4.2 K and (b) at T=45 K for the field direction $H\perp$ab-plane. Solid lines in the figures indicate the fitting curve by using Eq.(3). It is clear that the time dependence of the angle follows Eq.(3) and that ω and τ for T = 45 K are different from those for 4.2 K. At each temperature and magnetic field, k_{sample} and η_{sample} are obtained by using Eq.(2) and Eq.(4).

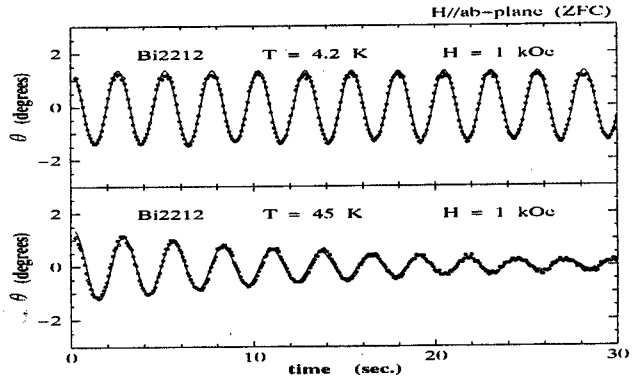

Fig. 2. Typical examples of the damping oscillations $\theta(t)$ for Bi2212. Solid lines indicate fitting curves by Eq.(3) in the text.

Figure 3 indicates the temperature dependence of torque coefficient k_{sample} in several magnetic fields. Figure 3 (a), (b), (c) and (d) correspond to the case Bi-1 (ZFC, $H\perp$ab), Bi-2 (FC, $H\perp$ab), Bi-3 (ZFC, H //ab) and Bi-4 (FC, H//ab), respectively. In the case of ZFC, $H\perp$ab (Fig. 3(a)), k_{sample} under field has negative sign and the magnitude increased abruptly below 20 K with decreasing temperature. The result is consistent with the increase of the static magnetic torque reported previously[15]. On the other hand, in the case of FC, $H\perp$ab (Fig. 3(b)), the k_{sample} is positive. It means that the flux pinning makes the field direction perpendicular to the ab-plane stable direction. For H//ab-plane , there is no difference in k_{sample} for ZFC (Fig. 3(c)) from k_{sample} for FC (Fig. 3(d)). k_{sample} be-

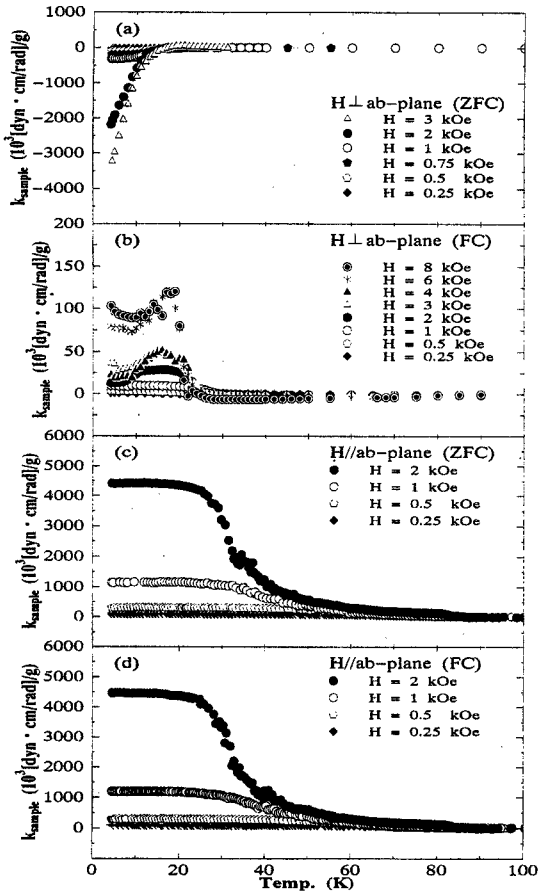

Fig. 3. Temperature dependence of torque coefficient k_{sample} in several magnetic fields for Bi2212. (a)Bi-1 case (ZFC, $H\perp$ab-plane), (b) Bi-2 case (FC, $H\perp$ab-plane),(c)Bi-3 case (ZFC, H//ab-plane) and (d) Bi-4 case (FC, H//ab-plane).

gins to increase slightly below T_c, increases rapidly at around 40 K, and then remains constant below 20 K. k_{sample} is proportional to H^2 in the temperature region where k_{sample} is independent of T below 20 K.

Temperature and field dependence of damping coefficient η_{sample} is obtained as shown in Fig. 4(a)(b) for the case Bi-1 (ZFC, $H \perp$ ab), Fig. 5(a)(b) for the case Bi-2 (FC, $H \perp$ ab), Fig. 6(a)(b) for the case Bi-3 (ZFC, H//ab) and Fig. 7(a)(b) for the case Bi-4 (FC, H//ab). Solid line in Fig. 4(b) and Fig. 5(b) for $H \perp$ ab-plane is the irreversibility line determined by the static magnetic torque measurements[16]. In the case of $H \perp$ ab-plane, as the temperature is decreases, η_{sample} increases, shows peaks with some complex structure in the irreversibility region in H-T plane as shown in Fig. 4 and 5. Since the oscillation damping in the irreversible region is observed in this experiments, it should be originated from the energy dissipation due to the depinning of the flux lines. Qualitatively, the data in FC is very similar to the data in ZFC. With increasing the field, η_{sample} increases abruptly around 1 kOe in the temperature range from 4.2 K to 30 K. In the case of H//ab-plane (Fig. 6 and 7), η_{sample} increases below T_c, shows a broad peak and decreases to zero with decreasing tem-

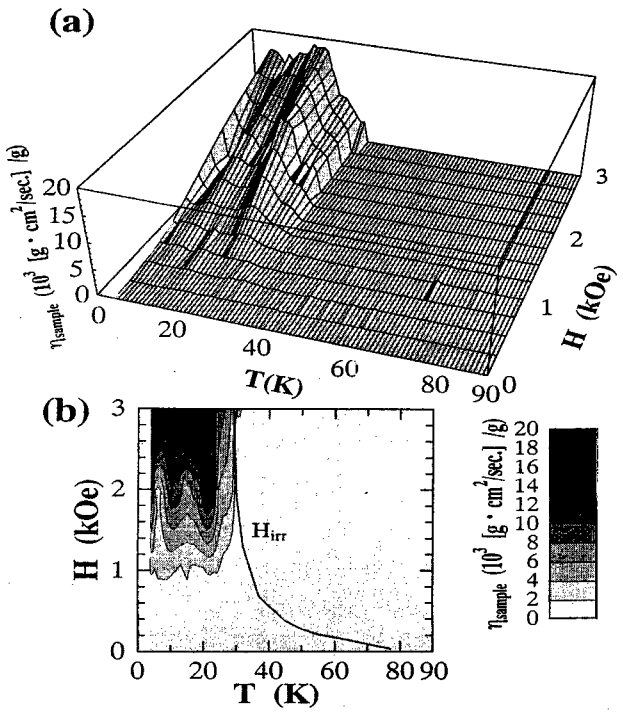

Fig. 4. Temperature and field dependence of η_{sample} in the case Bi-1 (ZFC, $H \perp$ ab-plane) for Bi2212. (a) 3D plotting, (b) Contour mapping.

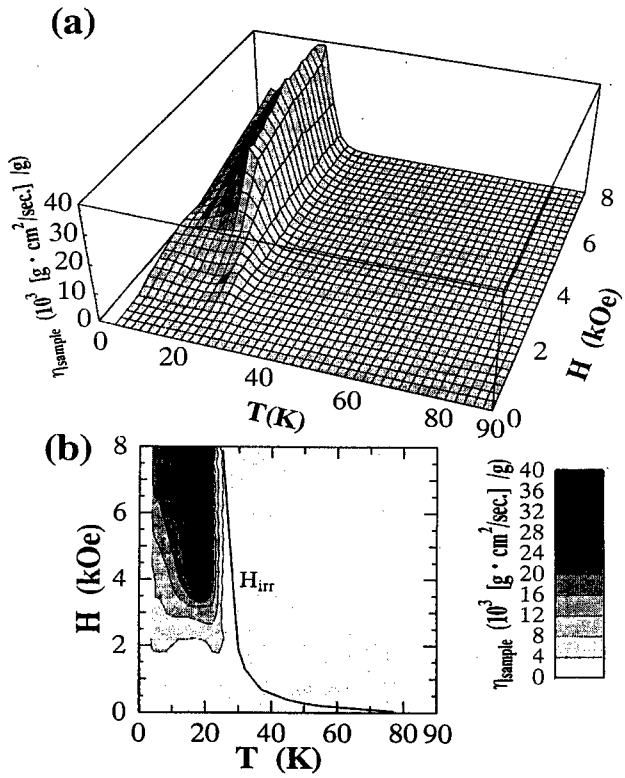

Fig. 5. Temperature and field dependence of η_{sample} in the case Bi-2 (FC, $H \perp$ ab-plane) for Bi2212. (a) 3D plotting, (b) Contour mapping.

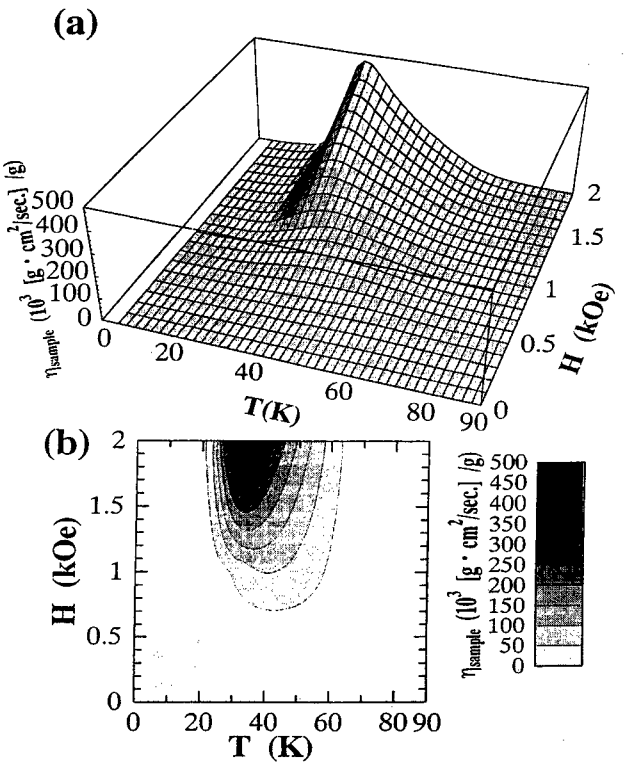

Fig. 6. Temperature and field dependence of η_{sample} in the case Bi-3 (ZFC, H//ab-plane) for Bi2212. (a) 3D plotting, (b) Contour mapping.

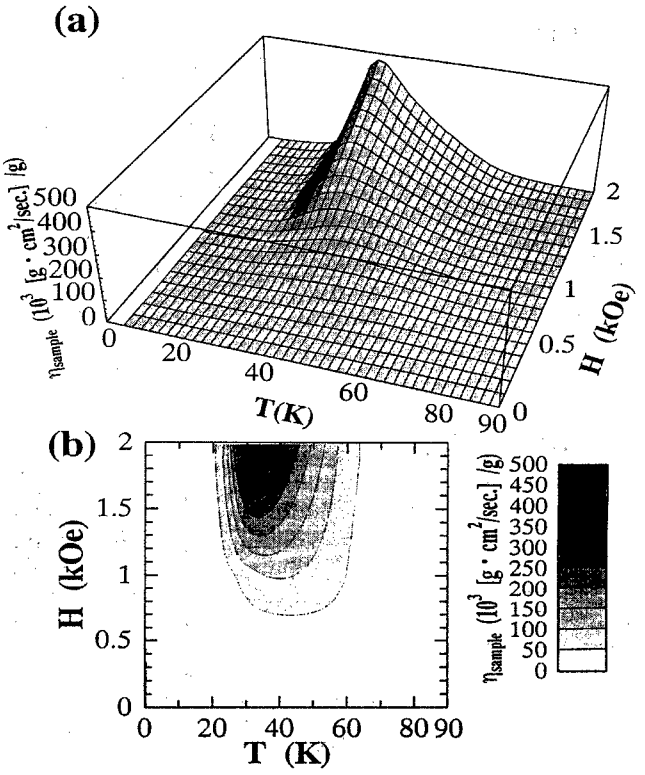

Fig. 7. Temperature and field dependence of η_{sample} in the case Bi-4 (FC, H//ab-plane) for Bi2212. (a) 3D plotting, (b) Contour mapping.

perature, while it remains finite at 4.2 K in the case $H\perp$ab-plane. The results are independent of the cooling method whether FC or ZFC.

3.2. κ-(BEDT-TTF)$_2$Cu(NCS)$_2$

Figure 8 indicates the temperature dependence of k_{sample} in several magnetic fields. Figure 8 (a), (b), (c) and (d) correspond to the case ET-1 (ZFC, $H\perp$bc), ET-2 (FC, $H\perp$bc), ET-3 (ZFC, H//bc) and ET-4 (FC, H//bc), respectively. In the case of FC, $H\perp$bc-plane (Fig. 8(b)), the k_{sample} is positive. It means that the flux pinning makes the field direction perpendicular to the bc-plane stable direction. In the case of ZFC, H//bc-plane (Fig. 8(c)), k_{sample} begin to increase slightly below T_c, increases rapidly at around 7 K, and then remains steadily below 2 K. At 2 K, k_{sample} is proportional to H^2.

Temperature and field dependence of damping coefficient η_{sample} is obtained as in Fig. 9(a)(b) in the case ET-1 (ZFC, $H\perp$bc), Fig. 10(a)(b) in the case ET-2 (FC, $H\perp$bc), Fig. 11(a)(b) in the case ET-3 (ZFC, H//bc) and Fig. 12(a)(b) in the case ET-4(FC, H//bc). Solid line in Fig. 9(b) and Fig. 10(b) for $H\perp$bc-plane is the irreversibility line determined by the static

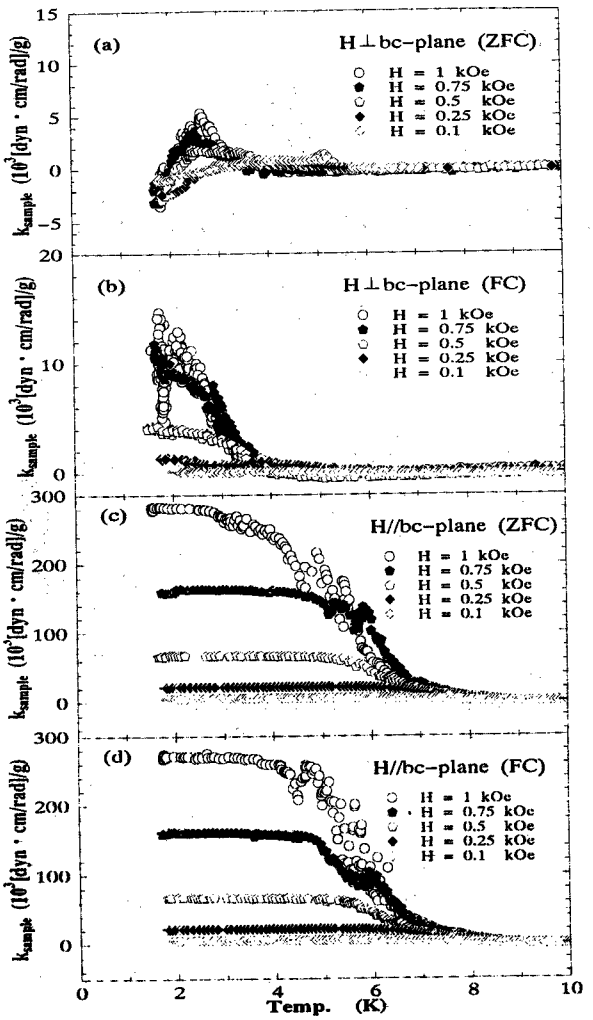

Fig. 8. Temperature dependence of torque coefficient k_{sample} in several magnetic fields for κ-(BEDT-TTF)$_2$Cu(NCS)$_2$. (a) ET-1 case (ZFC, $H\perp$bc-plane), (b) ET-2 case(FC, $H\perp$bc-plane), (c) ET-3 case(ZFC, H//bc-plane) and (d)ET-4 case(FC, H//bc-plane)

magnetic torque measurements[13]. In the case of $H\perp$bc-plane, as the temperature is decreases, η_{sample} increases, shows peaks with some structure in the irreversibility region in H-T plane as shown in Fig. 10. The oscillation damping is observed in the irreversible region as in the case of Bi2212. It suggests the energy dissipation due to the depinning of the flux lines. η_{sample} increases abruptly around 1 kOe with increasing the field in the temperature range from 1.8 K to 3 K. In the case of H//ab-plane (Fig. 11 and 12), the damping constant increases below T_c, shows a broad peak and decreases to zero with decreasing temperature, while it remains finite at 1.8 K in the case $H\perp$bc-plane.

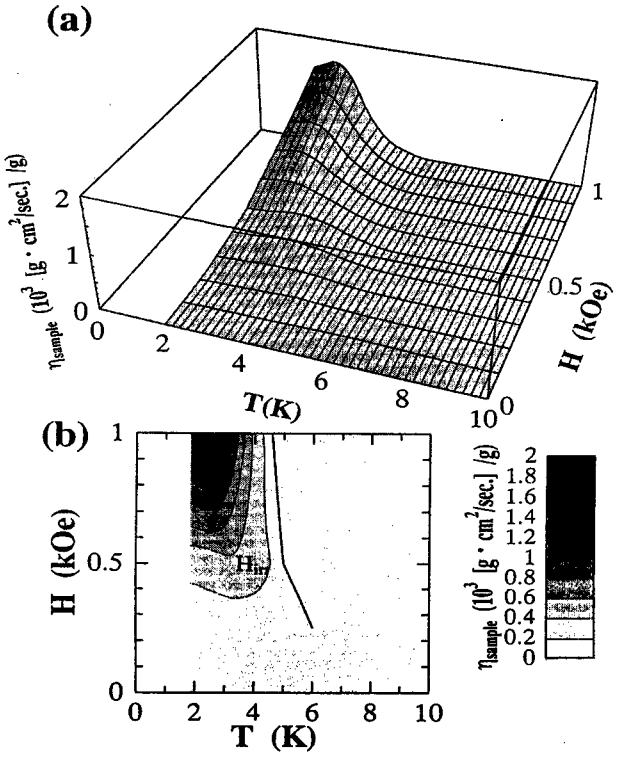

Fig. 9. Temperature and field dependence of η_{sample} in the case ET-1 (ZFC, $H \perp$ bc-plane) for κ-(BEDT-TTF)$_2$Cu(NCS)$_2$. (a) 3D plotting, (b) Contour mapping.

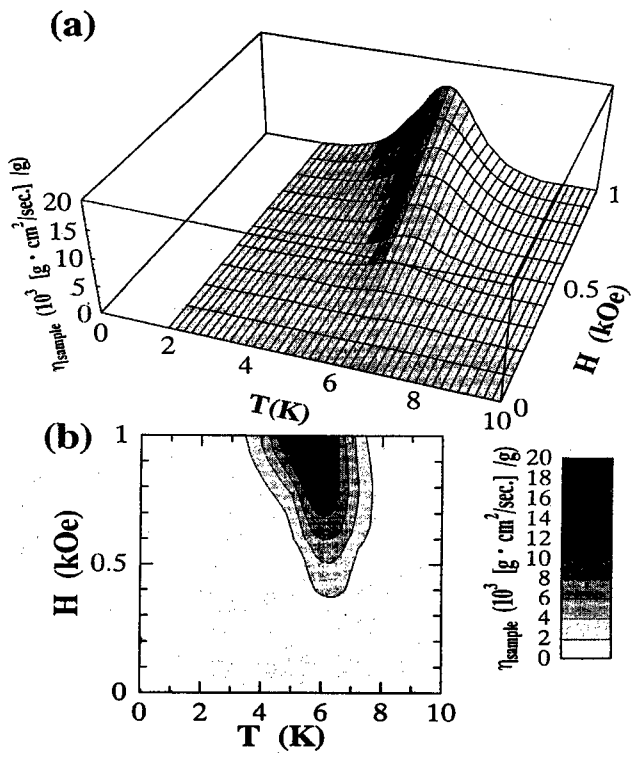

Fig. 11. Temperature and field dependence of η_{sample} in the case ET-3 (ZFC, H// bc-plane) for κ-(BEDT-TTF)$_2$Cu(NCS)$_2$. (a) 3D plotting, (b) Contour mapping.

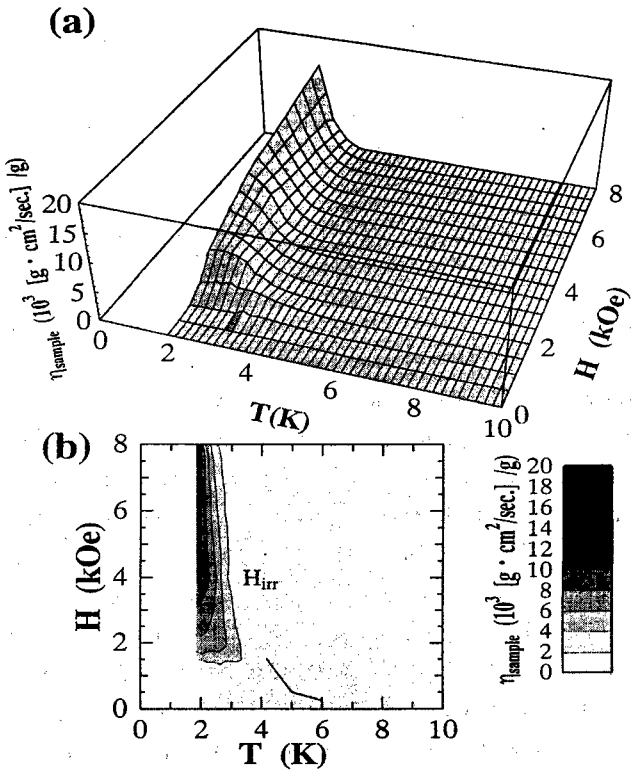

Fig. 10. Temperature and field dependence of η_{sample} in the case ET-2 (FC, $H \perp$ bc-plane) for κ-(BEDT-TTF)$_2$Cu(NCS)$_2$. (a) 3D plotting, (b) Contour mapping.

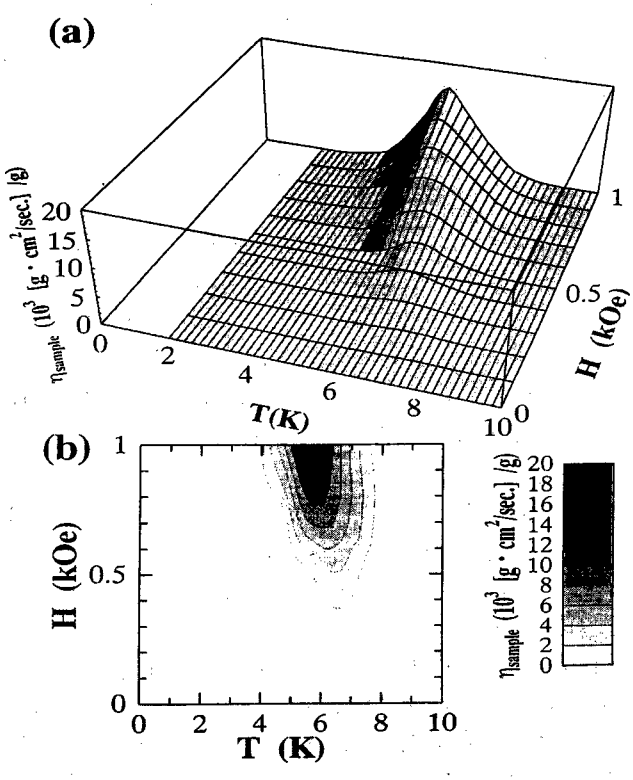

Fig. 12. Temperature and field dependence of η_{sample} in the case ET-4 (FC, H// bc-plane) for κ-(BEDT-TTF)$_2$Cu(NCS)$_2$. (a) 3D plotting, (b) Contour mapping.

3.3. Discussions

Bi2212 and κ-(BEDT-TTF)$_2$Cu(NCS)$_2$ are different kinds of superconductors. In Bi2212, the conduction is mainly carried in CuO_2 plane, while in κ-(BEDT-TTF)$_2$Cu(NCS)$_2$, it is contributed to the overlapping of the π-orbits in BEDT-TTF molecule layer. In addition, T_c for Bi2212 is ten times higher that for κ-(BEDT-TTF)$_2$Cu(NCS)$_2$. However, the results of dumping oscillation measurements are almost the same as a function of the reduced temperature, T/T_c. Therefor, the characteristic points of the experimental results are attributed to the common properties for highly two dimensional layered superconductors.

For highly two dimensional layered superconductors, the models of the vortex pancake[17] and the stepwise penetration[18] of magnetic flux perpendicular to the layer plane have been proposed. The flux parallel to the layer plane penetrates to spread into interlayer space. In the view point of this model, the common properties for these two superconducting materials are explained qualitatively.

Figure 13 (a) is the schematic diagram of flux penetration for the case of H perpendicular to the layer plane. The solid squares in the figure indicate the vortex pancakes. In this magnetic field configuration, the energy dissipation caused by displacement of the pancakes within the plane is observed in the torsional oscillation measurements.

Figure 13 (b) the schematic diagram of the flux penetration for the case of H parallel to the layer plane. In this magnetic field configuration, the magnetic flux can penetrate easily into the interlayer spacing without any resistance due to the extrinsic pinning effect. Therefor, no difference between the FC and ZFC cases is expected for both of k_{sample} and η_{sample}. In practice, the data for the FC case is the same as that for the ZFC case. In the low temperature region, the lock-in state where the flux which penetrate into one interlayer space can not move to the other interlayer space over the conducting layer is expected[19]. In such a state, since no flux can penetrate across the conducting layer, the magnetization perpendicular to the layer plane is proportional to the field component perpendicular to the layer plane as in the case of Meissner effect. Therefore, k_{sample} is expected to be proportional to H^2 because the torque is proportional to H^2 when the magnetization is proportional to H, and also η_{sample} is expected to be negligibly small. From the experimental results, the lock-in state is established below 20 K for Bi2212 and below 2 K for κ-(BEDT-TTF)$_2$Cu(NCS)$_2$.

At higher temperatures above the lock-in state, the direction of the flux changes when the applied field direction is tilted as indicated in Fig. 13 (b). The energy dissipation in the case of H parallel to the layer

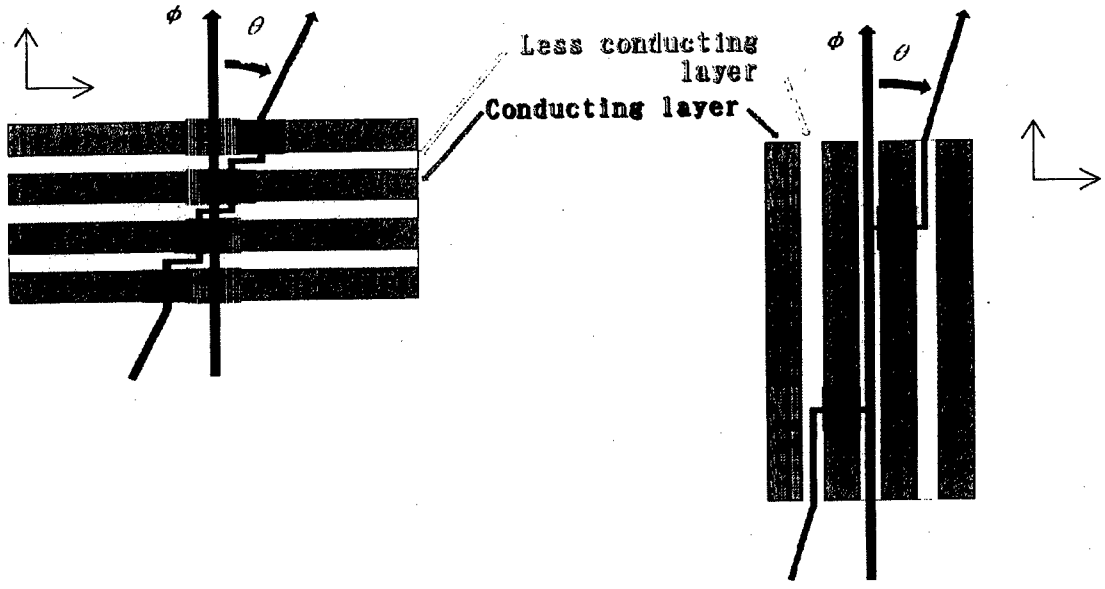

Fig. 13. Schematic diagram for the vortex pancake model for $H\perp$conducting layer (a) and that for $H//$conducting layer (b).

plane should be caused by creation and annihilation of the pancakes. This dissipation is anticipated to be much larger than that due to the displacement of the pancakes for the case of H perpendicular to the layer plane. This explains that the observed η_{sample} for H//layer-plane is ten times larger than that for $H\perp$ layer-plane.

In Fig. 4, 5 and 10, η_{sample} increases abruptly around 1 kOe with increasing the field in the temperature range from 4.2 to 30 K for Bi2212 and 1.8 to 3 K for κ-(BEDT-TTF)$_2$Cu(NCS)$_2$. This abrupt increase of energy dissipation may be related to the 3D-2D crossover of vortex pancakes[19].

4. Summary

Vortex state of oxide superconductor $Bi_2Sr_2CaCu_2O_{8+\delta}$ (Bi2212) and organic superconductor κ-(BEDT-TTF)$_2$Cu(NCS)$_2$ was investigated by free torsional oscillation in magnetic field. The temperature and field dependence of torque coefficient k_{sample} and the damping constant η_{sample} were obtained. Large anisotropy of damping constant was observed. It was explained by a model of the pancake vortex in layer superconductors.

References

1) E. H. Brant, Physica C 195(1992) 1-27
2) D. R. Nelson and H. S. Seung, Phys. Rev. B 39(1989) 9153
3) R. E. Hetzel, A. Sudb and D. A. Huse, Phys. Rev. Lett. 69(1992) 518
4) D. S. Fisher, M. P. A. Fisher and D. A. Huse, Phys. Rev. B 43(1991) 130
5) E. Zeldov, A. I. Larkin, V. B. Geshenbein, M. Konczykowski, D. Majer, B. Khaykovich, V. M. Vinokur and H. Shtrikman, Phys. Rev. Lett. 73(1994) 1428
6) E. Zerdov, D. Majer, M. Konczyknowski, V. B. Geshkenbein, V. M. Vinokur and H. Shtrikman, Nature 375(1995) 373
7) H. Safar, P. L. Gammel, D. A. Huse, D. J. Bishop, J. P. Rice and D. M. Ginsberg, Phys. Rev. Lett. 69(1992) 824
8) J. R. Clem, Phys. Rev. B43(1991) 7837
9) D, E. Farrell, J. P. Rice and D. M. Ginsberg, Phys. Rev. Lett. 67(1991)1165.
10) K. Okuda and S. Kawamata, JJAP 7(1992)279
11) D. E. Farrel, S. Bonham, J. Foster, Y. C. Chang, P. Z. Jiang, K. G. Vandervoort, D. J. Lam and V.G. Kogan, Phys. Rev. Lett. 63(1989)782
12) D. E. Farrel, C.J. Allen, R. C. Hadden and S.V. Chichester, Phys. Rev. B42(1990) 8694
13) S. Kawamata, K. Okuda, T.Sasaki, N.Toyota. Solid State Commun. 89(1994)955
14) T. Sasaki, H. Sato, N. Toyota. Solid State Commun. 76(1990)507.
15) S. Kawamata, N. Itoh, K. Okuda, T. Mochiku and K. Kadowaki, Physica C 195(1992)103.
16) H. Niimi, K. Inoue, S. Kawamata and K. Okuda, Physica C 235-240 (1994) 2637-2638.
17) M. Tachiki and S. Takahashi. Solid State Commun. 72(1989) 1083
18) M. Tachiki and S. Takahashi. Solid State Commun. 70(1989) 291
19) R. Cubitt, E. M. Forgan, G. Yang, S. L. Lee, D. McK. Paul, H. A. Mook, M. Yethiraj, P. H. Kes, T. W. Li, A. A. Menovsky, Z. Tarnawski and K. Mortensen, Nature 365(1993) 407.